

## Hydrothermal synthesis and enhanced sunlight photoactivity of Gd, N, and P tri-doped anatase-TiO<sub>2</sub> by TiCl<sub>4</sub> hydrolysis

Hongquan Jiang<sup>1\*</sup>, Mengdie Gao<sup>1</sup>, Shuying Zang<sup>2</sup>, Jingshen Li<sup>1</sup> & Xuefeng Wang<sup>1</sup>

<sup>1</sup>Key laboratory of Design and Synthesis of Functional Materials and Green Catalysis, Colleges of Heilongjiang Province, Harbin Normal University, Harbin 150025, PR China

<sup>2</sup>Key laboratory of Remote Sensing Monitoring of Geographic Environment, Colleges of Heilongjiang Province, Harbin Normal University, Harbin 150025, PR China

E-mail: h.q.jiang1119@163.com

Received 28 June 2014; accepted 16 July 2014

Gd, N, and P tri-doped anatase-TiO<sub>2</sub> (GNPTO) nano-photocatalyst has been synthesized from TiCl<sub>4</sub> hydrolysis using gadolinium nitrate, urea, and phosphoric acid as dopant sources via a hydrothermal process followed by calcination at 400°C. The physicochemical properties of as-synthesized samples have been investigated by X-ray diffraction, transmission electron microscopy, N<sub>2</sub> physical adsorption-desorption, X-ray photoelectron spectroscopy, Fourier transform infrared spectroscopy, UV-vis absorbance spectroscopy, and photoluminescence spectroscopy techniques. Doped P in the TiO<sub>2</sub> lattices plays a predominant role in inhibiting the phase transformation and crystal growth, and in improving the surface textural properties. Gd, N, and P tri-doping inhibits the recombination of photogenerated electrons and holes, increases the surface hydroxyls, and improves the UV absorption. GNPTO exhibits the highest photoactivity towards 4-chlorophenol (4-CP) degradation under simulated sunlight irradiation among the undoped, doped, and P25 TiO<sub>2</sub>. ·OH radicals play a key role in 4-CP degradation, and photogenerated electrons also play a minor role through the final formation of ·OH via H<sub>2</sub>O<sub>2</sub>. Synergetic mechanism of the enhanced photoactivity for GNPTO has also been discussed.

**Keywords:** Gd, N, and P tri-doping, Hydrolysis, Photocatalysis, Synergetic effect, Titanium dioxide, TiCl<sub>4</sub>

Titania nanomaterials have attracted tremendous attention due to their applications in environmental remediation and renewable energy sources<sup>1,2</sup>. However, TiO<sub>2</sub> has two major drawbacks, including its relatively large energy band gap (3.2 eV for the anatase phase), which hampers exploitation of solar light in photocatalytic reactions, and low quantum efficiency, because of high recombination rate of photogenerated electron-hole pairs<sup>3,4</sup>. So far, the efficient utilization of solar energy and improvement of quantum efficiency are still the greatest technical challenges for its environmental applications.

Doping with p-block anions or metal ions has been largely pursued to sensitize TiO<sub>2</sub> toward visible light and to favor the electron-hole separation<sup>1,4</sup>. Specially, co-doped TiO<sub>2</sub> systems have been paid great attention. For example, Liu *et al.*<sup>5</sup> synthesized Gd and N co-doped TiO<sub>2</sub> nanotubes by hydrothermal method and ion-exchanging, which exhibited significantly enhanced photocatalytic activities under visible light irradiation. Lin *et al.*<sup>6</sup> prepared phosphorus and nitrogen co-doped TiO<sub>2</sub> by a modified sol-gel method,

of which the photoactivities under both UV and visible light were further improved. Recently, an effective strategy has been developed to enhance the visible light activity of TiO<sub>2</sub> by a synergetic effect of rare earth (Yb, Sm or Pr), N and P tri-doping<sup>7-9</sup>. Previously, Gd, C, N and P quaternary-doped TiO<sub>2</sub> was synthesized using tetrabutyl titanate as precursor and absolute ethyl alcohol as solvent via a modified sol-solvothermal process<sup>10</sup>, where tetrabutyl titanate was more expensive than inorganic precursors like TiCl<sub>4</sub> or Ti(SO<sub>4</sub>)<sub>2</sub>, and an additive organic solvent such as ethanol was needed. As a result, a lot of residual carbon still presented in the heat-treated samples, even though the subsequent calcination at 550 °C was carried out to remove surface organic remainders and to improve crystallinity.

In present work, Gd, N, and P tri-doped anatase-TiO<sub>2</sub> nano-photocatalyst was synthesized by hydrolysis of a cheaper TiCl<sub>4</sub> using gadolinium nitrate, urea, and phosphoric acid as dopant sources via a hydrothermal process. The influence of Gd, N and P on the physicochemical properties and

photocatalytic performances of TiO<sub>2</sub> was investigated. A possible synergetic mechanism was also discussed based on the results of corresponding characterization and active species trapping experiments.

## Experimental Section

### Preparation of photocatalysts

Gd, N, and P tri-doped anatase-TiO<sub>2</sub> nano-photocatalyst was prepared by a hydrothermal method using a cheaper TiCl<sub>4</sub> as precursor. In a typical procedure, 4 mL of TiCl<sub>4</sub> was dissolved in 10 mL of 1.43 mol/L HCl solution in an ice-water bath to form solution A. The solution containing 0.0334 g of Gd(NO<sub>3</sub>)<sub>3</sub>·6H<sub>2</sub>O (the mass percentage of Gd<sup>3+</sup> in the theoretical TiO<sub>2</sub> powder was 0.4 wt.%), 0.5466 g of urea (the mol ratio of Ti:N was 2:1), and 18 mL of distilled water was added dropwise to solution A under vigorous stirring to form solution B. Then the mixture solution of 0.5 mL of 2.92 mol/L phosphoric acid (the mass percentage of P in the theoretical TiO<sub>2</sub> powder was 1.56 wt.%) and 7.5 mL of distilled water was added dropwise into the solution B. The resulting mixture was stirred continuously for 60 min, and then transferred into 50 mL Teflon-lined stainless steel autoclave. The sealed autoclave was heated at 160°C for 3 h for hydrothermal treatment, followed by naturally cooling to room temperature. The obtained powder was filtered, washed with distilled water, dried in oven at 110°C for 12 h, and then calcined at 400°C for 0.5 h. The Gd, N, and P tri-doped sample was denoted as GNPTO.

For comparison, the co-doped, single-doped, and un-doped TiO<sub>2</sub> were prepared by the same procedures except for the difference of dopants. Gd and N co-doped, N and P co-doped, Gd-doped, N-doped, P-doped, and non-doped TiO<sub>2</sub> were denoted as GNTO, NPTO, GTO, NTO, PTO, and TO, respectively.

### Characterization

X-ray diffraction (XRD) patterns of all samples were characterized in the range of 10-90° (2θ) by a Japan Shimadzu XRD-6000 X-ray diffractometer with Cu Ka radiation (λ = 0.15418 nm). The crystallite size was calculated by the Scherrer equation [Eq. (1)]:

$$D = \frac{K\lambda}{\beta \cos \theta} \quad \dots (1)$$

where, *D* is the crystalline size, *K* is the constant usually taken as 0.89, λ is the wavelength of X-ray radiation (0.15418 nm), and β is the full width at half

maximum (FWHM) after subtraction of equipment broadening, and θ is the diffraction angle. The lattice distortion was also estimated from the XRD spectrum using the formula [Eq. (2)]:

$$\varepsilon = \frac{\beta}{4 \tan \theta} \quad \dots (2)$$

where ε is the lattice distortion. The morphology was observed with a FEI Tecnai G<sup>2</sup>TF20 transmission electron microscopy (TEM) at an accelerating voltage of 200 kV. Brunauer-Emmett-Teller (BET) surface areas, pore volumes and average pore sizes of the samples were determined from N<sub>2</sub> adsorption isotherms at 77 K using the Quantachrome NOVA2000E specific surface area analyzer after the samples had been degassed in the flow of N<sub>2</sub> at 180°C for 3 h.

X-ray photoelectron spectroscopy (XPS) measurements were recorded on a PHI-5700 (ESCA System) instrument with Al Ka radiation (*hν* = 1486.6 eV). The binding energies of all investigated elements were calibrated with the C1s peak at 284.6 eV for the adventitious carbon. Fourier-transform infrared spectra (FT-IR) of the samples were collected using a VERTEX 80 FT-IR spectrometer between the frequency range of 4000-400 cm<sup>-1</sup> using KBr as diluent.

Ultraviolet-visible absorbance spectra of the samples were recorded with a Shimadzu UV-2550 spectrophotometer equipped with an integrating sphere using BaSO<sub>4</sub> as the reference standard at room temperature in air. Photoluminescence (PL) spectra of the samples were measured with a Hitachi F-4500 fluorescence spectrophotometer at room temperature using He-Cd laser as an excitation light source. The excitation wavelength was 325 nm.

### Photoactivity measurements

The photoactivities of the samples were evaluated by the degradation of 4-CP in aqueous solution under simulated sunlight irradiation similar to the method in our report<sup>9-11</sup>. Photocatalytic experiments were carried out in a 250 mL of photochemical glass reactor with an external cooling jacket to ensure the experiments carried out at room temperature. A 500 W high-pressure Xenon lamp made in China was placed at about 35 cm above the solution surface as simulated sunlight source, and a heat insulation glass was fixed between the light source and solution surface. In a typical photocatalytic experiment, 80 mg of the

photocatalyst was dispersed in 100 mL of 4-CP solution (20 mg/L) by ultrasonic bath for 15 min in dark. Prior to irradiation, the suspension was magnetically stirred in the dark for 30 min to ensure the establishment of an adsorption/desorption equilibrium. At 30 min intervals of irradiation, about 4 mL of the suspension was taken and centrifuged at 8000 rpm for 15 min. The concentration of 4-CP in supernatant liquid was analyzed by recording the absorbance at 225 nm using a UV-2550 spectrophotometer. The solution and the centrifuged powders were then added back to the reactor.

To investigate the mineralization of 4-CP by GNPTO, the total organic carbon (TOC) was analyzed using a Shimadzu total organic carbon analyzer (TOC-VCPN).

## Results and Discussion

### Structural properties

Figure 1 shows the XRD patterns of as-prepared samples via the hydrothermal process followed by

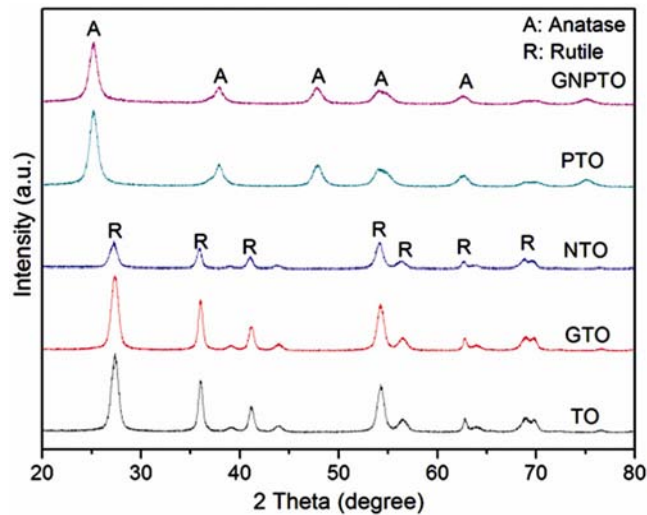


Fig. 1 — XRD patterns of TO, GTO, NTO, PTO, and GNPTO calcined at 400°C.

calcination at 400°C. Only diffraction peaks of rutile TiO<sub>2</sub> are observed for TO, GTO, and NTO samples. Compared with TO, Gd or N single-doping results in broadening the (110) peaks of rutile phase and decreasing their intensities, indicating that Gd or N single-doping can efficiently inhibit the growth of TiO<sub>2</sub> nanocrystallites. In contrast, as for PTO and GNPTO, only the diffraction peaks of anatase TiO<sub>2</sub> are observed, implying that P-doping plays a predominant role in inhibiting the phase transformation of TiO<sub>2</sub> from anatase to rutile. No Gd, N and P derived peaks are observed probably due to the high dispersion or too low doping contents of the dopants.

The average crystallite sizes calculated by Scherrer's equation and lattice distortion degrees estimated are given in Table 1. As shown in Table 1, phosphorus plays a superior role in inhibiting the crystal growth of TiO<sub>2</sub> to gadolinium and nitrogen. The lattice distortions of the doped samples increase in the order of PTO > GNPTO > GTO > NTO > TO, confirming that the doping atoms have incorporated into the TiO<sub>2</sub> lattices.

GNPTO observed by TEM presents regular elliptic nanosheets with a diameter of about 12×16 nm. The selected area electron diffraction (SAED) reveals that GNPTO exists as polycrystallites of anatase TiO<sub>2</sub>. HRTEM image of the lattice fringes displays that the spacing between the lattice fringes is 0.35 nm, corresponding to the (101) planes of anatase TiO<sub>2</sub>.

Figure 2 presents the N<sub>2</sub> adsorption-desorption isotherms and pore size distributions of as-synthesized samples. As shown in Fig. 2(a), PTO and GNPTO exhibit the isotherms of type IV with type H2 hysteresis loops at a relative pressure range of 0.5-0.97, but TO, GTO and NTO show the isotherms of type II with type H2 hysteresis loops at a relative pressure range of 0.5-0.97, indicating that all

Table 1 — Physicochemical properties of TO, GTO, NTO, PTO, and GNPTO calcined at 400°C.

Sample	Crystallite size (nm)	(101) Interplanar distance (nm)	Distortion of lattice $\epsilon$	$S_{\text{BET}}$ (m <sup>2</sup> /g)	Pore volume (cm <sup>3</sup> /g)	Pore size (nm)
TO	42.17 <sup>a</sup>	3.2453 <sup>c</sup>	0.00089	26.6	0.1078	9.56
GTO	32.46 <sup>a</sup>	3.2453 <sup>c</sup>	0.00115	26.4	0.1014	9.58
NTO	35.89 <sup>a</sup>	3.2476 <sup>c</sup>	0.00105	30.2	0.1020	12.43
PTO	9.59 <sup>b</sup>	3.5145 <sup>d</sup>	0.03827	121.4	0.3638	5.60
GNPTO	15.34 <sup>b</sup>	3.5009 <sup>d</sup>	0.01562	105.1	0.3046	5.64

<sup>a</sup>Average crystal size is calculated from rutile (110) peak.  
<sup>b</sup>Average crystal size is calculated from anatase (101) peak.  
<sup>c</sup>Rutile (110) interplanar spacing.  
<sup>d</sup>Anatase (101) interplanar spacing.

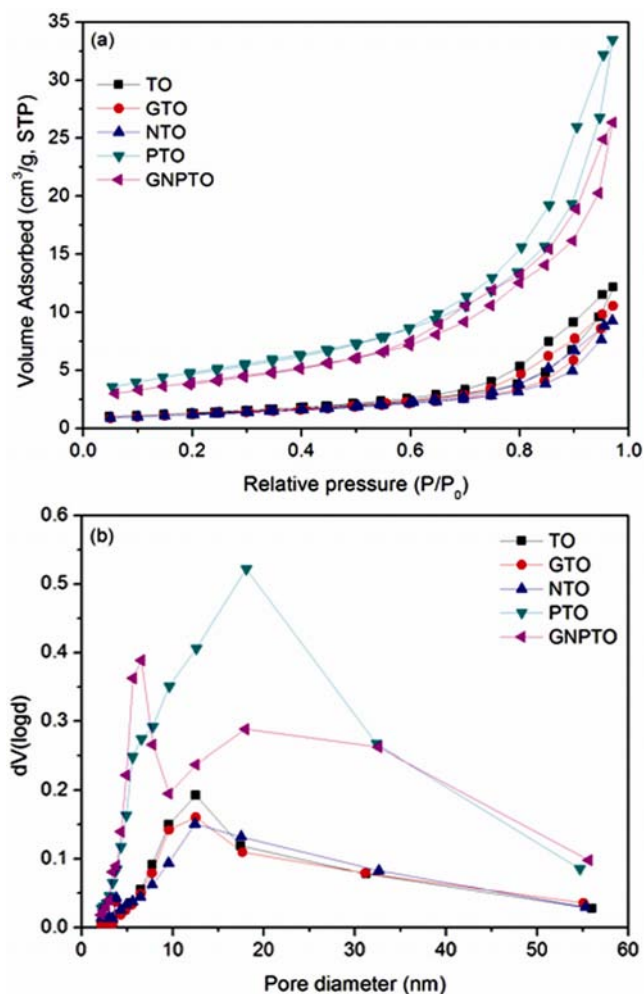


Fig. 2 — (a) N<sub>2</sub> adsorption-desorption isotherms and (b) pore size distributions of TO, GTO, NTO, PTO, and GNPTO.

samples contain heterogeneous slit-shaped mesopores. These mesopores are from the aggregation of primary nanosheets<sup>12</sup>. The pore size distributions of the samples determined by the BJH method are shown in Fig. 2(b). It is clear that only PTO has a broad unimodal distribution, other samples show bimodal distributions.

The BET surface areas, pore volumes, and pore sizes of the samples are summarized in Table 1. It is seen that Gd or N single-doping has a little effect on the surface textural properties of TiO<sub>2</sub>. However, P-doping significantly increases the BET surface area from 26.6 m<sup>2</sup>/g of TO to 121.4 m<sup>2</sup>/g, and increases the pore volume from 0.1078 cm<sup>3</sup>/g of TO to 0.3638 cm<sup>3</sup>/g, and decreases the pore diameter from 9.56 nm of TO to 5.60 nm. GNPTO displays BET surface area of 105.1 m<sup>2</sup>/g, pore volume of 0.3046 cm<sup>3</sup>/g, and an average pore diameter of 5.64 nm. Clearly, P atoms in

TiO<sub>2</sub> lattices play a fateful role in improving the surface textural properties.

#### Chemical composition

The characteristic peaks of nitrogen element in the N 1s XPS spectrum of GNPTO are weak due to low N-doping concentration. However, four contributions at 399.1 eV, 400.9 eV, 403.5 eV and 405.2 eV are still observed at least. The peak at 399.1 eV is assigned to the substitutional nitrogen in N–Ti–O structure, whose binding energy increases compared to N 1s peak at 396–397 eV corresponding to Ti–N bond<sup>13</sup>, because of the decrease in the electron density on the nitrogen due to higher electronegativity of oxygen than that of nitrogen. The peak at 400.9 eV corresponds to chemisorbed NH<sub>x</sub>-containing compounds<sup>14</sup>. The peak at 403.5 eV and 405.2 eV may be due to molecularly adsorbed nitrogen containing compounds NO<sub>2</sub><sup>-</sup> and NO<sub>3</sub><sup>-</sup>, respectively, on the surface<sup>13–15</sup>.

In the P 2p XPS spectrum of GNPTO, a peak at 134.2 eV is attributed to the chemisorption of orthophosphate<sup>16</sup>, indicating that P atoms are probably incorporated as cations. When P<sup>5+</sup> replaces Ti<sup>4+</sup> in TiO<sub>2</sub> lattices to form P–O–Ti bond, the electron density on Ti decreases, and then the binding energy of Ti positively shifts.

The peaks of Ti 2p<sub>3/2</sub> and Ti 2p<sub>1/2</sub> for GNPTO are centered at 459.1 and 464.75 eV, implying that Ti exists as Ti (IV) oxidation state. Compared to that of pure TiO<sub>2</sub> (458.4 eV)<sup>8</sup>, the Ti 2p<sub>3/2</sub> binding energy of GNPTO shifts toward a higher binding energy about 0.7 eV, which mainly results from the formation of Ti–O–P linkages, decreasing the electron density of Ti and increasing the binding energy. No Gd 4d peak at 142.1 eV is observed because its doping concentration is too low to be detected.

The asymmetric peak of O 1s XPS spectra for GNPTO is fitted into two peaks. The main peak at 530.35 eV corresponds to the bulk oxygen in Ti–O bond. The minor peak at 532.06 eV is attributed to the presence of hydroxyl oxygen<sup>17</sup>. The surface hydroxyl content in GNPTO evaluated by the XPS analysis is 22.09%, confirming that a large number of surface hydroxyl groups exist in GNPTO. This can be further confirmed by the next FTIR analysis.

The broad absorption peak around 3404 cm<sup>-1</sup> in the FTIR spectrum of GNPTO is assigned to stretching vibration of structure hydroxyl groups bonding to titanium atoms<sup>13</sup>. However, no peak around 3404 cm<sup>-1</sup> is observed in that of TO. Therefore, Gd, N, and P tri-

doping obviously increases the surface hydroxyl concentration of TiO<sub>2</sub>. Similar result also was obtained in our previous report<sup>10</sup>. The origin should be mainly ascribed to the following two aspects. On the one hand, the doped Gd<sup>3+</sup> ions with special 4f<sup>7</sup> electron configuration are beneficial to form complexes with various Lewis bases including surface hydroxyl. It has also been validated by Zhao *et al.* that Gd-doping benefits the adsorption of the surface hydroxyl groups<sup>18</sup>. On the other hand, the charge imbalance from P<sup>5+</sup> substitution of Ti<sup>4+</sup> is compensated by the decrease in the oxygen vacancy and the increase in the surface hydroxyl group.

In addition, the peaks at 1626 cm<sup>-1</sup> correspond to the bending vibration of physically adsorbed water molecules on the sample surface<sup>13,19</sup>. The absorption peak at 1046 cm<sup>-1</sup> for GNPTO is observed, further confirming that P mainly exists as Ti—O—P bond<sup>7,8</sup>. The absorption bands from 1000 cm<sup>-1</sup> to 400 cm<sup>-1</sup> are related to the stretching vibration of Ti—O—Ti<sup>11</sup>. The peaks around 2920 cm<sup>-1</sup> and 2841 cm<sup>-1</sup> are assigned to the stretching vibration of =CH<sub>2</sub><sup>15,20</sup>, which can be attributed to adsorbed organic contaminants on the surface because of no carbon sources in the precursors of TO.

### Optical properties

Figure 3 shows the UV-vis absorbance spectra of TO, GTO, NTO, PTO, and GNPTO and plot of  $(\alpha h\nu)^{1/2}$  versus light energy in the inset. It is worth mentioning that GNPTO exhibits the strongest UV absorption intensity among all samples, which will contribute to the improvement of the UV

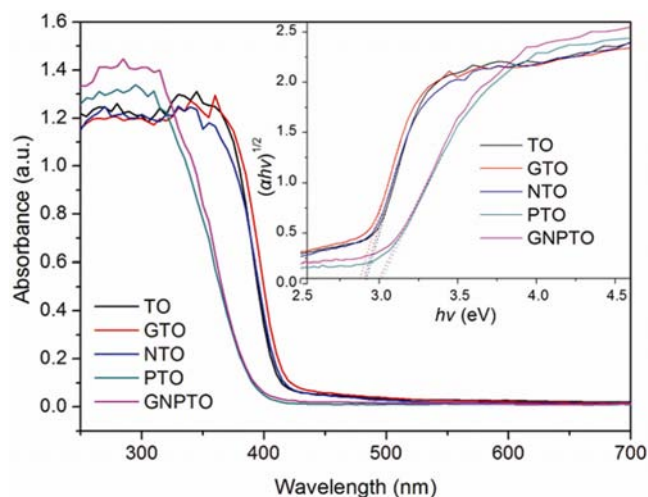


Fig. 3 — UV-vis absorbance spectra of TO, GTO, NTO, PTO, and GNPTO and plot of  $(\alpha h\nu)^{1/2}$  versus light energy (inset).

photoactivity. As observed, TO, GTO, and NTO extend their absorption edges into the visible region over 400 nm. GTO and NTO exhibit a little red shift of the absorption edge as compared with TO, indicating that Gd or N single-doping decreases the band gap energy of TiO<sub>2</sub>. The oxygen vacancies introduced by Gd<sup>3+</sup> substitution of Ti<sup>4+</sup> in TiO<sub>2</sub> lattices are responsible for the reduction of the band gap energy, and then the optical absorption edge of GTO is shifted to the visible light region<sup>21</sup>. The substitutional N and interstitial N for NTO induce the formation of localized occupied states in the gap, which results in the red shift of absorbance edge<sup>22</sup>. In contrast, P-doping leads to a obvious blue shift of the absorption edge owing to both a higher band gap energy of anatase than that of rutile and the quantum size effect from a smaller crystallize size of PTO (9.59 nm) than that of TO (42.17 nm). GNPTO exhibits a little red shift compared with PTO, but obvious blue shifts in comparison with GTO and NTO, which is ascribed to a cooperative effect of Gd, N, P-tridoping. As shown in Figure 3 inset, the band gap energies of TO, GTO, NTO, PTO, and GNPTO are 2.92, 2.88, 2.90, 3.02, and 3.0 eV, respectively. The band gap energy (3.02 eV) of PTO is much lower than that of anatase TiO<sub>2</sub> (3.2 eV), indicating that P-doping can reduce the energy gap of anatase TiO<sub>2</sub>, which is ascribed to the valence band (VB) is spanned by mixing the P 3p states with O 2p states<sup>7,8</sup>.

Figure 4 shows the PL spectra of TO, GTO, NTO, PTO, and GNPTO at the excitation wavelength of 325 nm. PL emission results from the recombination of excited electrons and holes, the lower PL intensity indicates the lower recombination rate of electrons

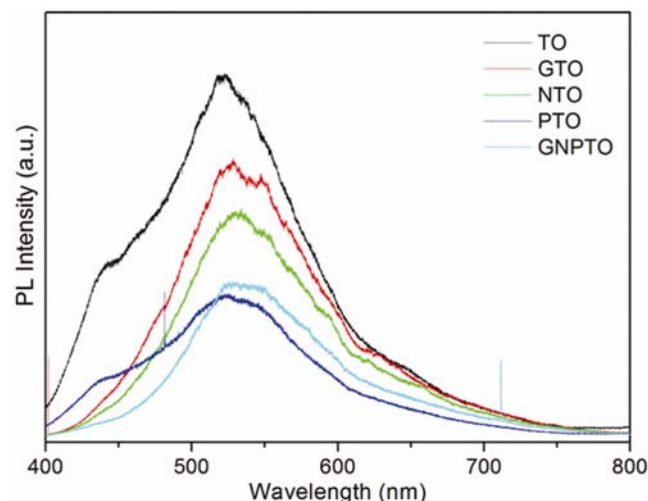


Fig. 4 — PL spectra of TO, GTO, NTO, PTO, and GNPTO.

and holes<sup>23</sup>. Gd, N or P single-doping significantly lowers PL spectrum intensity of TiO<sub>2</sub> in the order of TO > GTO > NTO > PTO, indicating that the single-doping inhibits the radiative recombination of photogenerated electrons and holes. However, GNPTO presents a much lower PL intensity than PTO under 517 nm and a little higher PL intensity than PTO over 517 nm. As a result, Gd, N, and P tri-doping further inhibits the recombination of photogenerated electrons and holes. Based on the results of XRD analysis, we think that the origin of inhibitive recombination is partly assigned to the crystal distortion, which prolongs the lifetime of photogenerated carriers and promotes the separation of photogenerated carriers. Additionally, the charge imbalance by P<sup>5+</sup> substitution of Ti<sup>4+</sup> is compensated by additional surface hydroxyl groups or the reduction of oxygen vacancies<sup>11</sup>, which can also contribute to the inhibitive effect.

#### Effect and mechanism discussion of doping on the photoactivity of TiO<sub>2</sub>

##### Comparison of photocatalysts

The photoactivities of the non-doped and doped TiO<sub>2</sub> were evaluated by 4-CP degradation under simulated sunlight irradiation. No direct photolysis of 4-CP was observed under sunlight irradiation, implying no self-sensitized degradation. The adsorption tests of 4-CP in dark showed that the adsorption for 4-CP on all samples was negligible. The photocatalytic degradation of 4-CP over different photocatalysts under simulated sunlight irradiation increases in the order of NTO < GTO < GNTO < TO < P25 < PTO < NPTO < GNPTO. According to the results of XRD and UV-vis absorbance spectra analysis, the decreased photoactivities of N and/or Gd doped samples result primarily from the lower redox potentials of the electron and hole generated under simulated sunlight irradiation. However, P-doping significantly increases the photoactivity of TiO<sub>2</sub>. As expected, GNPTO exhibits the highest photoactivity among all samples, which is much superior to that of P25, confirming that a synergetic effect on the improvement of photoactivity is produced by Gd, N, and P tri-doping.

When 20 mg/L 4-CP solution is exposed to simulated sunlight irradiation in the presence of 0.8 g/L GNPTO, the absorption of 4-CP decreases rapidly with increasing irradiation time and almost disappears after 90 min, and no new absorption bands appear in either visible or ultraviolet region,

indicating that 4-CP has been decomposed completely. The removal rate of TOC reaches 93.6% after irradiation for 120 min, which further confirms the mineralization of 4-CP. However, the TOC removal delays to a certain degree in comparison with 4-CP decomposition, implying the formation of organic intermediates in the photocatalytic oxidation process. The complete mineralization will be achieved after the irradiation of a longer time.

##### Synergetic mechanism

In general, the photoinduced reactive species such as h<sup>+</sup>, ·OH, and ·O<sub>2</sub><sup>-</sup> are suspected to be involved in the photocatalytic reaction<sup>24</sup>. The effects of KI, CH<sub>3</sub>OH, dissolved oxygen, and K<sub>2</sub>S<sub>2</sub>O<sub>8</sub> on 4-CP degradation in the GNPTO suspensions under simulated sunlight irradiation were investigated to scrutinize the main reactive species. As shown in Fig. 5(a), When 50 mM

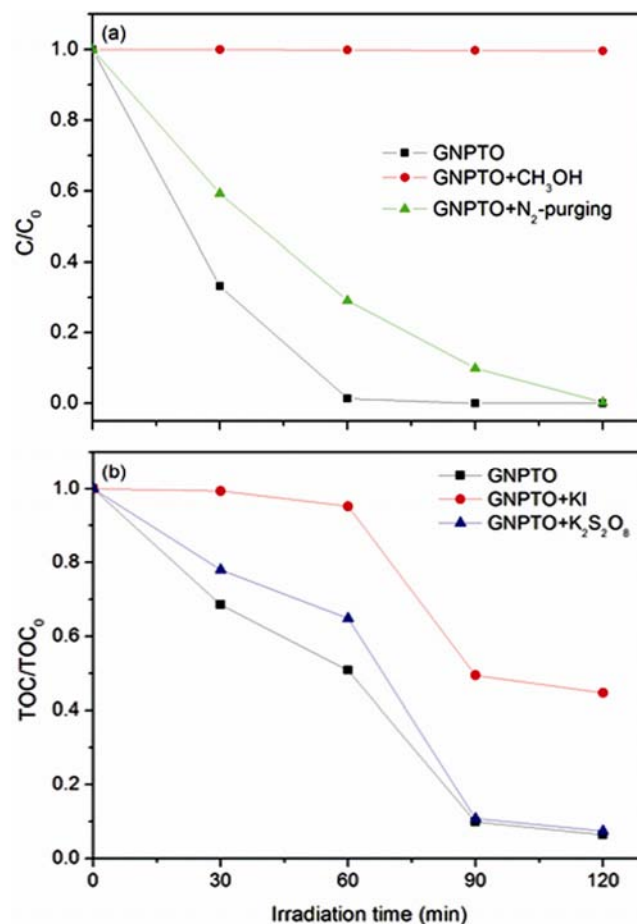


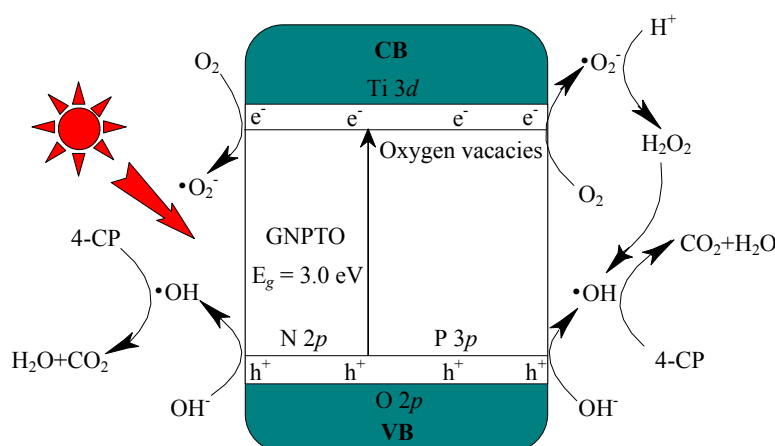
Fig. 5 — Comparison of the 4-CP removal (a) and TOC reduction (b) in the presence of GNPTO under simulated sunlight irradiation with scavengers in air equilibrium systems, without scavengers in an air equilibrium system, and without scavengers in a N<sub>2</sub>-purged system. Initial 4-CP concentration, 20 mg/L; catalyst dosage, 0.08 g/L; reaction temperature, 25°C.

CH<sub>3</sub>OH (CH<sub>3</sub>OH, a scavenger for ·OH radicals in the solution)<sup>25,26</sup> is added into the GNPTO suspension, no degradation of 4-CP occurs under simulated sunlight irradiation. It can be concluded that ·OH radicals play a key role towards the degradation of 4-CP in the GNPTO suspension under simulated sunlight irradiation. The level of dissolved oxygen is reduced from 0.15 mM to 0.01 mM by N<sub>2</sub>-purging<sup>27,28</sup>. The amount of 4-CP removal is obviously reduced by N<sub>2</sub>-purging in comparison with the case of air equilibrium, demonstrating that the dissolved oxygen acts as an acceptor of photogenerated e<sup>-</sup>, retarding the recombination of photogenerated e<sup>-</sup>/h<sup>+</sup> through the formation of reactive species ·O<sub>2</sub><sup>-</sup>.

As shown in Fig. 5(b), the TOC reduction of 4-CP is significantly inhibited upon the addition of a 10-fold molar concentration (with respect to the initial 4-CP concentration) KI (Iodide ion, a scavenger for hole and adsorptive ·OH). However, the TOC reduction of 4-CP is also reduced by adding a 10-fold molar concentration of K<sub>2</sub>S<sub>2</sub>O<sub>8</sub> (a more efficient electron acceptor)<sup>28</sup>. The photogenerated electron is transferred to the surface adsorbed O<sub>2</sub> to form superoxide radical anion (·O<sub>2</sub><sup>-</sup>), and transform further to hydroxyl radical (·OH)<sup>29,30</sup>. According to no degradation of 4-CP when adding 50 mM methanol, we conclude that it is ·OH other than ·O<sub>2</sub><sup>-</sup> that directly attacks target pollutant 4-CP, and ·O<sub>2</sub><sup>-</sup> can be further protonated to form ·OH at last, and then partake the degradation of 4-CP<sup>11</sup>.

Based on the above results, the possible mechanism for the enhanced photocatalytic activity of GNPTO towards the degradation of 4-CP can be described as Scheme 1. The N 2p and P 3p energy levels above the

valence band of anatase TiO<sub>2</sub> and the oxygen vacancy energy level below its conduction band cooperate to narrow the band gap to 3.0 eV. Under simulated sunlight irradiation with energy larger than 3.0 eV, electrons in the valence band (VB) of GNPTO can be excited to the conduction band (CB), and the same amount of holes can be created in the VB. The photogenerated holes can be captured by the surface hydroxyl of GNPTO to form active species ·OH radicals, which are known to be the most oxidizing species<sup>30</sup>. As demonstrated, ·OH radicals play a major role in the degradation of 4-CP over GNPTO. Meanwhile, the photogenerated electrons in the CB can be captured by the surface adsorbed O<sub>2</sub> to yield ·O<sub>2</sub><sup>-</sup> radicals, which can immediately react with H<sup>+</sup> ions to generate H<sub>2</sub>O<sub>2</sub>, further converting into ·OH radicals<sup>31,32</sup>. The generated ·OH radicals in the solution attack target pollutant 4-CP molecules and lead to its hydroxylation, oxidation, ring opening, and finally mineralization into CO<sub>2</sub>, H<sub>2</sub>O, and inorganic ions<sup>3</sup>. In fact, only a small number of electrons and holes usually participate in photocatalytic reactions, while others recombine. Gd, N, and P tri-doping leads to the enhanced UV absorption, implying that the formation of more photogenerated carriers, which are favorable for the enhanced photoactivity. Gd, N, and P tri-doping further inhibits the recombination of photogenerated electrons and holes, which results in more charge carrier forming reactive species, and then promotes the degradation of 4-CP. Gd, N, and P tri-doping increases the surface hydroxyls, which are beneficial to photocatalytic process. The hydroxyl groups may accept photogenerated holes, producing strong oxidative hydroxyl free radicals (·OH), and the



Scheme 1 — A possible mechanism for the enhanced photocatalytic activity of GNPTO towards the degradation of 4-CP.

surface hydroxyl groups can also act as adsorption centers for O<sub>2</sub>, CO and organic molecules. In addition, the presence of P in the crystal lattices plays a predominant role in inhibiting the phase transformation from anatase to rutile and the crystal growth, as well as in improving the surface textural properties of TiO<sub>2</sub>. All above aspects contribute to the enhanced photoactivity of GNPTO.

### Conclusion

- 1 Base on TiCl<sub>4</sub> hydrolysis, a hydrothermal method followed by the calcination at 400°C has been successfully developed to prepare Gd, N, and P tri-doped anatase-TiO<sub>2</sub> nanosheets using gadolinium nitrate, urea, and phosphoric acid as dopant sources. A synergetic effect is produced by Gd, N, and P tri-doping. Under simulated sunlight irradiation, Gd, N, and P tri-doped TiO<sub>2</sub> achieves an excellent photocatalytic performance much superior to commercial P25 TiO<sub>2</sub>. It is a promising high-performance photocatalyst for environmental application.
- 2 OH radical is main active species in the photocatalytic degradation process of 4-CP by GNPTO. Photogenerated electron also plays a minor role, which can react with adsorbed O<sub>2</sub> to produce reactive ·O<sub>2</sub><sup>-</sup>, and be further protonated to form final ·OH, and then partake the degradation of 4-CP.
- 3 Doped P in the crystal lattices plays a predominant role in inhibiting the phase transformation from anatase to rutile and the crystal growth, as well as in improving the surface textural properties of TiO<sub>2</sub>. The N 2p and P 3p energy levels above the valence band of anatase TiO<sub>2</sub> and the oxygen vacancy energy level below its conduction band cooperate to narrow the band gap to 3.0 eV. Gd, N, and P tri-doping further inhibits the recombination of photogenerated electrons and holes, increases the surface hydroxyls, and improves the UV absorption ability. The enhanced photoactivity for the tri-doped TiO<sub>2</sub> is attributed to the synergetic effect of the reduced recombination of charge carriers, increased surface hydroxyls, enhanced UV absorption, and well crystalline anatase structure, as well as improved surface textural properties.

### Acknowledgement

This work was financially supported by the National Nature Science Foundation of China

(No.41030743), the Nature Science Foundation of Heilongjiang Province (No.E201323), the Harbin Special Fund for Innovation Talents of Science and Technology (No.2013RFXXJ081) and the Science and Technology Research Program of Education Bureau of Heilongjiang Province (No.12531213).

### References

- 1 Park H, Park Y, Kim W & Choi W, *J Photochem Photobiol C*, 15 (2013) 1.
- 2 Lalitha K, Durga Kumari V & Subrahmanyam M, *Indian J Chem*, 53A (2014) 472.
- 3 Aziz R A & Sopyan I, *Indian J Chem Technol*, 20 (2013) 137.
- 4 Dozzi M V & Selli E, *J Photochem Photobiol C*, 14 (2013) 13.
- 5 Liu H, Liu G, Xie G, Zhang M, Hou Z & He Z, *Appl Surf Sci*, 257 (2011) 3728.
- 6 Lin L, Zheng R Y, Xie J L, Zhu Y X & Xie Y C, *Appl Catal B: Environ*, 76 (2007) 196.
- 7 Jiang H Q, Yan P P, Wang Q F, Zang S Y, Li J S & Wang Q Y, *Chem Eng J*, 215-216 (2013) 348.
- 8 Jiang H Q, Wang Q Y, Zang S Y, Li J S & Wang Q F, *J Hazard Mater*, 261 (2013) 44.
- 9 Jiang H Q, Wang Q F, Li S Y, Li J S & Wang Q Y, *Chin J Catal*, 35 (2014) 1068.
- 10 Wang Q Y, Jiang H Q, Zang S Y, Li J S & Wang Q F, *J Alloys Compd*, 586 (2014) 411.
- 11 Jiang H Q, Wang Q F, Zang S Y, Li J S & Wang X F, *J Alloys Compd*, 600 (2014) 34.
- 12 Wang Z Y, Lv K L, Wang G H, Deng K J & Tang D G, *Appl Catal B: Environ*, 100 (2010) 378.
- 13 Pang Y L & Abdullah A Z, *Chem Eng J*, 214 (2013) 129.
- 14 Gago R, Redondo-Cubero A, Vinnichenko M, Lehmann J, Munnik F & Palomares F J, *Mater Chem Phys*, 136 (2012) 729.
- 15 Joshi M M, Labhsetwar N K, Mangrulkar P A & Tijare S N, *Appl Catal A: Gen*, 357 (2009) 26.
- 16 Mäkie P, Persson P & Österlund L, *J Colloid Interface Sci*, 392 (2013) 349.
- 17 Munuera G, Gonzalez-Elipse A R, Espinos J P & Navio A, *J Mol Struct*, 143 (1986) 227.
- 18 Zhao D, Peng T Y, Liu M, Lu L L & Cai P, *Microporous Mesoporous Mater*, 114 (2008) 166.
- 19 Li Y S, Jiang F L, Xiao Q, Li R, Li K, Zhang M F, Zhang A Q, Sun S F & Liu Y, *Appl Catal B: Environ*, 101 (2010) 118.
- 20 Ho C H, Shieh C Y, Tseng C L, Chen Y K & Lin J L, *J Catal*, 261 (2009) 150.
- 21 Chen W, Yuan P, Zhang S, Sun Q, Liang E & Jia Y, *Physica B*, 407 (2012) 1038.
- 22 Di Valentin C, Finazzi E, Pacchioni G, Selloni A, Livraghi S, Paganini M C & Giamello E, *Chem Phys*, 339 (2007) 44.
- 23 Toyoda T, Hayakawa T & Shen Q, *Mater Sci Eng B*, 78 (2000) 84.
- 24 Yang Y Q, Zhang G K, Yu S J & Shen X, *Chem Eng J*, 162 (2010) 171.

- 25 Li F T, Zhao Y, Hao Y J, Wang X J, Liu R H, Zhao D S & Chen D M, *J Hazard Mater*, 239-240 (2012) 118.
- 26 Zhu X Q, Zhang J L & Chen F, *Appl Catal B: Environ*, 102 (2011) 316.
- 27 Song S, Hong F Y, He Z Q, Cai Q L & Chen J M, *J Colloid Interface Sci*, 378 (2012) 159.
- 28 He Z Q, Wang C, Wang H Y, Hong F Y, Xu X H, Chen J M & Song S, *J Hazard Mater*, 189 (2011) 595.
- 29 Dai G P, Liu S Q, Liang Y, Liu H J & Zhong Z C, *J Mol Catal A: Chem*, 368-369 (2013) 38.
- 30 Cheng X W, Yu X J, Li B Y, Yan L, Xing Z P & Li J J, *Mater Sci Eng B*, 178 (2013) 425.
- 31 Wang J, Wang P, Cao Y, Chen J, Li W, Shao Y & Zheng Y, *Appl Catal B: Environ*, 136-137 (2013) 94.
- 32 Bubacz K, Kusiak-Nejman E, Tryba B & Morawski A W, *J Photochem Photobiol A*, 261 (2013) 7.